Article

# Automated Construction of Potential Energy Surfaces Suitable to Describe van der Waals Complexes With Highly-Excited Nascent Molecules: The Rotational Spectra of Ar–CS($v$) and Ar–SiS($v$)

Ernesto Quintas-Sánchez, Richard Dawes, Kelvin Lee, and Michael C McCarthy

*J. Phys. Chem. A*, **Just Accepted Manuscript** • DOI: 10.1021/acs.jpca.0c02685 • Publication Date (Web): 05 May 2020

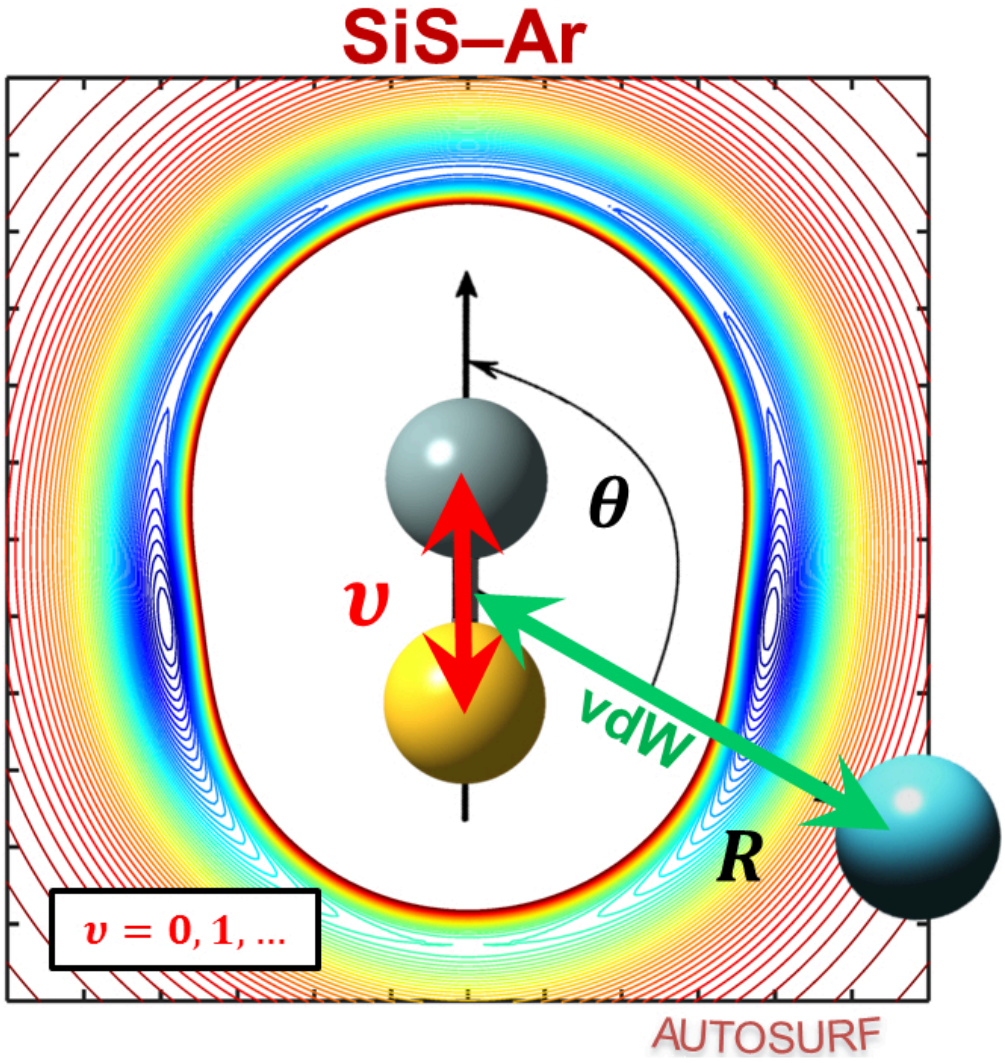


111x118mm (150 x 150 DPI)

# Automated Construction of Potential Energy Surfaces Suitable to Describe van der Waals Complexes with Highly-Excited Nascent Molecules: The Rotational Spectra of Ar–CS($v$) and Ar–SiS($v$)

Ernesto Quintas-Sánchez and Richard Dawes*

*Department of Chemistry, Missouri University of Science and Technology, Rolla, Missouri 65409, United States*

Kelvin Lee

*Harvard-Smithsonian Center for Astrophysics, Cambridge, MA 02138, United States*

Michael C. McCarthy*

*Harvard-Smithsonian Center for Astrophysics, Cambridge, MA 02138, United States and School of Engineering and Applied Sciences, Harvard University, 29 Oxford Street, Cambridge, MA 02138, United States*

(Dated: May 4, 2020)

*Corresponding authors, email: dawesr@mst.edu; mmccarthy@cfa.harvard.edu

# Abstract

Some reactions produce extremely hot nascent-products which nevertheless can form sufficiently long-lived van der Waals (vdW) complexes—with atoms or molecules from a bath gas—as to be observed via microwave spectroscopy. Theoretical calculations of such unbound resonance-states can be much more challenging than ordinary bound-state calculations depending on the approach employed. One encounters not only the floppy, and perhaps multi-welled potential energy surface (PES) characteristic of vdWs complexes, but in addition must contend with excitation of the intramolecular modes and its corresponding influence on the PES. Straightforward computation of the (resonance) rovibrational levels of interest, involves the added complication of the unbound nature of the wavefunction, often treated with techniques such as introducing a complex absorbing potential. Here, we have demonstrated that a simplified approach of making a series of vibrationally effective PESs for the intermolecular coordinates—one for each reaction product vibrational quantum number of interest—can produce vdW levels for the complex with spectroscopic accuracy. This requires constructing a series of appropriately weighted lower-dimensional PESs for which we use our freely available PES-fitting code AUTOSURF. The applications of this study are the Ar–CS and Ar–SiS complexes, which are isovalent to Ar–CO and Ar–SiO, the latter of which we considered in a previously reported study. Using a series of vibrationally effective PESs, rovibrational levels and predicted microwave transition frequencies for both complexes were computed variationally. A series of shifting rotational transition frequencies were also computed as a function of the diatom vibrational quantum number. The predicted transitions were used to guide and inform an experimental effort to make complementary observations. Comparisons are given for the transitions that are within the range of the spectrometer and were successfully recorded. Calculations of the rovibrational level pattern agree to within 0.2 % with experimental measurements.

## I. INTRODUCTION

The Ar–CO complex has been extensively studied both theoretically and experimentally and can by now be considered the prototypical heavy atom-diatom complex.[1–5] Recently, we reported a combined theoretical/experimental study of Ar–SiO,[6] isovalent to Ar–CO but with some interesting differences. The initial motivation to study SiO came from its relevance to astrochemistry, as its radio emission lines are observed from a number of astronomical sources.[7–11] SiO is a reactive species and can be formed as a hot nascent reaction product. Indeed, the previous study reported observation of lines attributable to at least 12 quanta in the Si–O stretch ($v_{\mathrm{SiO}} = 12$).[6] This presents some challenges for a theoretical treatment. The excited diatom, with a huge excess of internal energy—on the order of 100 times greater than the rare-gas-complex binding energy—nevertheless forms sufficiently long-lived complexes as to be observed via microwave spectroscopy. This means that in principle, the states of interest are metastable resonances, which for a theoretical treatment can necessitate approaches such as adding a complex absorbing potential to the Hamiltonian. In the previous study, we showed that the coupling between the inter- and intra-molecular modes is so weak, and the lifetimes of the complexes so long, that the approximation of a vibrationally averaged (over the probability density of the excited diatom) potential energy surface (PES) describing the intermolecular coordinates, is remarkably accurate. Thus, for each level of diatom excitation, a separate calculation may proceed as for an ordinary set of bound rovibrational levels. This can still be challenging however, since the complex may be very floppy or even have multiple isomers. Moreover, with respect to the electronic structure method employed to construct the PES, large distortions of the excited diatom could require a multireference description, within which it is difficult (prohibitively expensive) to capture the high-order electron correlation often necessary to compute non-bonded interactions accurately.

Here, we describe the extension of our approach to two more systems from the same set of isovalent species: Ar–CS and Ar–SiS. The diatoms of this series (without complexation by a rare gas atom) have received some attention of their own in the past.[12] The dipole moment of CO famously defies expectations based on electronegativity differences, and its dipole, though small (0.1 D), has the polarity $C^-O^+$. More generally, the CO dipole function—changing with the bond distance—passes through zero near equilibrium, such

that its expectation value changes sign (flips direction) upon excitation by several quanta of vibration. Harrison analyzed the dipole moment functions of the series CO, SiO, CS, and SiS from the point of view of competing charge and induced atomic dipole contributions.[12] In this light, CS is perhaps more remarkable than CO, since despite a nearly negligible difference in atomic electronegativities, the measured dipole is quite large (1.96 D) and is also polarized as $C^-S^+$. The other two members of the series, SiO and SiS, have dipoles of 3.1 and 1.7 D respectively and are oppositely polarized as $Si^+O^-$ and $Si^+S^-$.[13,14] The four species also exhibit a significant range of bond distances and effective sizes, polarizabilities, etc., all of which could affect the nature of the rare-gas binding potential and hence the formation of such complexes, their structures, and dynamics. We report here new high quality PESs for the Ar–CS and Ar–SiS systems, constructed at the CCSD(T)-F12b/CBS level of *ab initio* theory, as a function of the level of diatom vibrational excitation. We also report predicted rovibrational transitions for the Ar–CS and Ar–SiS complexes, comparing with new experimental measurements, and discuss them in terms of characterization of the PESs and comparison with the Ar–CO and Ar–SiO systems.

In Section II we describe the theoretical methodology, beginning with the PES construction, and followed by the methods employed to compute the rovibrational states. In Section III a description of the experimental methods and apparatus is given. In Section IV, a discussion and characterization of the PES and derived states, including predicted transition frequencies and comparison with experiments is given. The conclusion and relations between the members of the isovalent series is given in Section V.

## II. THEORETICAL CALCULATIONS

As illustrated in Figure 1, to describe the vdW complexes formed by a rare gas atom C and a more strongly-bound diatomic molecule AB we choose Jacobi coordinates, for which the Hamiltonian is well known.[15] As can be seen in the figure, $r$ represents the interatomic coordinate of the molecule AB, while $R$ describes the distance between the center-of-mass of the AB subunit and the atom C. Typically to compute spectra of these complexes, one would need the full 3D PES for the system: $V(r, R, \theta)$. However, given the difference in intra- *vs.* inter-molecular vibrational frequencies (typically on the order of 100 fold), a simplified approach that has proven to be very accurate[6] is to make a vibrationally-

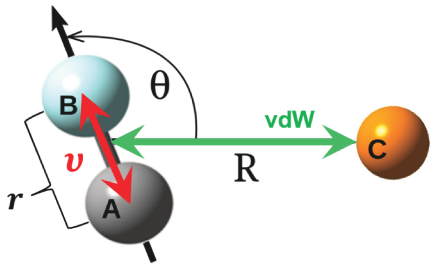


FIG. 1. Internal (Jacobi) coordinate system used to describe a generic AB–C system. See the text for details.

averaged PES (averaged over the probability densities of the AB vibrational states) for the interatomic coordinates of the molecule (one PES for each vibrational quantum number of interest). These vibrational-level-specific PESs can then be used to study the rovibrational states of the system, and their progression, as a function of the number of vibrational quanta $v$ in the molecule AB. This allows the vdW rovibrational states of interest—for a particular AB diatomic vibrational quantum number—to be computed as bound states on the corresponding 2D PES (avoiding complications such as introducing complex absorbing potentials, traditionally used to compute resonances). As mentioned in the introduction, the energy of even one quantum of excitation in the diatom will usually exceed the vdW complex binding energy, and with several quanta, perhaps greatly so.

The vibrationally-averaged PES, $V_v(R,\theta)$, can be obtained by solving:

$$V_v(R,\theta) = \langle \Psi_v(r)|V(r,R,\theta)|\Psi_v(r)\rangle = \int |\Psi_v(r)|^2 V(r,R,\theta)dr \ , \tag{1}$$

where $\Psi_v(r)$ represents the wave function associated with the vibrational quantum number $v$ of molecule AB. Conveniently, this integral can be solved numerically. A particularly accurate methodology is to use a potential optimized discrete variable representation (PO-DVR) of the PES,[16–19] which is so efficient that—as we will show later—only a few points in the coordinate $r$ are needed to obtain good convergence of the integral. This way, equation 1 can be reduced to:

$$V_v(R,\theta) = \sum_{i=1}^{n} C_v(r_i) V_{r_i}(R,\theta) \ , \tag{2}$$

where the weights $C_v(r_i)$ correspond to the PO-DVR representation (using $n$ points) of the wave function $\Psi_v(r)$, and the $V_{r_i}$ are a series of 2D PESs corresponding to each PO-DVR point $r_i$: $V_{r_i}(R,\theta) = V(r_i,R,\theta)$.

The general procedure can be summarized as follows: First, a 1D *ab initio* potential energy curve for the molecule AB is computed, with a grid of points dense enough to be smoothly interpolated and a range of interatomic distance $r$ adequate to calculate the number of diatomic energy levels of interest. Then, the discrete variable representation (DVR) method[16–19] can be used to compute the vibrational energy levels and the corresponding wave functions. Next, the lowest $n$ diatomic vibrational probability densities can be represented using $n$ PO-DVR points—to obtain the weights $C_v(r_i)$, *cf.* equation 2—and for each of the $n$ PO-DVR coordinates $\{r_i\}$, a 2D PES $V_{r_i}(R,\theta)$ should be constructed to represent the vdW interactions in the AB–C system. Finally, the vibrationally-averaged PES for any given set of intermolecular coordinates $(R,\theta)$ can be obtained by simply evaluating equation 2.

It is worth pointing out that some of the fundamental components of this procedure, such as constructing effective interaction PESs for various excitations of the monomers, and employing a PO-DVR to compute rovibrational levels have been used for several decades.[20–22] Here, combining these methods with automation, parallel high-performance computing, and highly accurate quantum chemistry methods, has culminated in a robust, efficient procedure with predictive spectroscopic accuracy, requiring minimal human effort.

### A. Automated construction of 2D PESs

In order to construct the chosen number of reduced dimensional PESs, we make use of our automated code AUTOSURF.[23] For the present applications, as well as the previously reported Ar–SiO system, in each case we used eight points in the diatomic coordinate, which implies eight separate 2D PESs $V_{r_i}(R,\theta)$, each constructed by fixing the diatomic bond distance at a particular value of the PO-DVR grid point. Having eight 2D PESs permits one to compute rovibrational levels for vibrationally averaged AB($v = 0$–7), as well as perform rigorous 3D calculations for AB($v = 0$). Our interpolative approach to PES construction, implemented in AUTOSURF, has been described before in detail[24,25] and is freely available.[23] It computes and fits *ab initio* data in prespecified ranges of coordinates and energy, and in a fully automated fashion, iteratively refines the PES by adding data until a prespecified level of fitting accuracy is reached. It is interfaced to popular electronic structure codes and will set up and run calculations at any specified level of theory, including composite methods or protocols. Here, for the Ar–CS and Ar–SiS systems, we used the MOLPRO code[26] to

generate energies at the CCSD(T)-F12b/CBS(VTZ-F12,VQZ-F12) level, extrapolated to the CBS limit with the $l^{-3}$ formula.[25,27]

### B. Rovibrational calculations

To compute the rovibrational levels and wavefunctions, the RV3 three-atom variational code of Wang and Carrington was used.[28] RV3 implements a parallel symmetry-adapted Lanczos algorithm and a numerically exact kinetic energy operator in various possible chosen sets of coordinates. The parity-adapted rovibrational basis is a product of stretch and shared-K bend-rotation basis functions (more details have been provided previously).[28] RV3 permits specification of total angular momentum $J$ and parity and also provides wavefunction and probability density plotting, making assignment and interpretation relatively straightforward. Before performing a series of 2D calculations for AB($v$) with the set of vibrationally averaged 2D PESs, an initial 3D calculation was performed. The 3D calculation was performed with a product basis in such a way as to permit use of the $n$ 2D PESs, computed at different $r_{\mathrm{AB}}$ bond distances (not the vibrationally averaged ones). For the $r_{\mathrm{AB}}$ stretching coordinate, the same $n$ PO-DVR points were used, such that the existing $n$ 2D PESs could be called in the 3D calculations. For the vdW stretch coordinate $R$, 200 sine DVR functions were used and for the angle, the $l_{\mathrm{max}}$ value in the Legendre basis was set to 120 (for a total of 192,000 functions). This rather large basis converges the low-lying levels to better than $10^{-4}\,\mathrm{cm}^{-1}$. Low-lying (the first 10) vibrational levels for $J = 0$–10 were computed.

## III. EXPERIMENT

Experiments were conducted at the Center for Astrophysics, using a combination of chirped-pulse[29] and cavity[30] Fourier transform microwave spectroscopies. Both spectrometers have been described in previous publications,[31,32] so only details specific to this study are highlighted here. Briefly, CS and SiS were produced by co-expanding $CS_2$ and $SiH_4$, heavily diluted in Ar ($\sim$1%), while applying an voltage potential (1 kV) between two closely-spaced copper electrodes in the throat of a supersonic jet source; the backing pressure behind the nozzle was of 2.5 kTorr. This arrangement has been used with considerable success to detect

a wide array of reactive species including silicon-bearing species such as Si(H)SiH[33] and silicon-oxides HOSiOH.[34] As the gas mixture exits the discharge assembly, it rapidly undergoes supersonic expansion, resulting in substantial cooling of the internal degrees of freedom of the products. Collisional cooling is most efficient for rotation, resulting in rotational temperatures of only a few K near the center of the chamber. Owing to combined effects of collisional excitation by electrons, the use of atomic buffer gases, and a relatively short transit time thru the discharge source, vibrational degrees of freedom are poorly quenched in the expansion, resulting in vibrationally temperatures that can range from hundreds to several thousand K.[35,36] As a result, rotational transitions from vibrationally excited states are common, especially so for diatomics because their vibrational frequencies greatly exceed typical collision frequencies.

Since Ar−SiO,[37] Ar−CS,[38] and SiS[39] have been studied previously, the experimental conditions (*e.g.*, discharge voltage, gas mixing ratios, timings) were adjusted to optimize production of each species. For Ar−SiO, trace contamination of atmospheric $O_2$ was sufficient to produce this complex in high abundance in the presence of silane, while a source of sulfur ($CS_2$) was required for the other two species. For each species, line intensities were first maximized using a cavity-enhanced (5–26 GHz) spectrometer, and then a broadband chirped-pulse (8–18 GHz) spectrum was immediately acquired. Each spectrum is an average of roughly 1.3 million shots, collected at a rate of 10 chirps per gas pulse at a gas pulse repetition rate of 6 Hz ($\sim$ 6 hours). To identify Ar-containing features, a second spectrum was collected under nominally the same experimental conditions using Ne rather than Ar as the buffer gas. After data collection, the spectra were analyzed using PySpecTools, an open-source Python library for performing interactive and reproducible analysis of rotational spectra.[40,41]

## IV. RESULTS

### A. Vibrationally averaged PESs

At the CCSD(T)-F12b/CBS level, the well-depths of the Ar–CS and Ar–SiS interaction are 136 $cm^{-1}$ and 160 $cm^{-1}$ respectively—while their harmonic constants are 1285.08 $cm^{-1}$ and 749.64 $cm^{-1}$ respectively—which means that as expected, vdW states for vibrationally

excited ($v > 0$) diatoms in the Ar–CS and Ar–SiS complexes are resonances, rather than bound states. Thus, to study the rovibrational states of the complexes, and their progressions as a function of the number of vibrational quanta in the CS and SiS subunits (as described in Section II), a series of eight different 2D PESs were constructed for each system. This allows the vdW rovibrational states of interest for a particular diatomic vibrational quantum number $v$ to be computed as bound states on the corresponding 2D vibrationally averaged PES.

First, a 1D potential energy curve for CS and SiS was computed at the CCSD(T)-F12b/CBS level of theory. The lowest ($J = 0$) vibrational energy levels, computed using the DVR method, are shown in the Supporting Info (SI), Table S1. The corresponding experimentally fitted anharmonic progression is also shown in the table. Next, the lowest eight diatomic vibrational probability densities were represented using eight PO-DVR points corresponding to CS (SiS) bond distances distributed between $r_{\rm CS} = 1.409$ and $r_{\rm CS} = 1.731$ Å ($r_{\rm SiS} = 1.803$ and $r_{\rm SiS} = 2.131$ Å). Table S2, in the SI, provides the precise PO-DVR point locations, as well as the relative weights given to each PES—coefficients $C_v(r_i)$ in equation 2—in order to construct the vibrationally averaged PESs for CS($v = 0$–3) and SiS($v = 0$–3). The corresponding expectation values of the $r_{\rm CS}$ and $r_{\rm SiS}$ coordinates: $\langle\Psi_v|r_{AB}|\Psi_v\rangle$, used in the vdW rovibrational calculations, are also given in Table S2.

For each of the eight CS and SiS bond distances (PO-DVR points), a separate 2D PES was constructed for each system using AUTOSURF, for the coordinate range: $2.4 < R < 15.0$ Å and $0 < \theta < \pi$ ($R$, $\theta$, as defined in Figure 1). Table S3 (in the SI), provides some details concerning the construction and accuracy of each individual PES. As can be seen in the table, on the order of 200 *ab initio* points were always sufficient to converge the root-mean-square (RMS) fitting error below 0.07 $\rm cm^{-1}$ for energy-regions below the asympote ($E < E_{asymp}$). Despite the similar topography of the eight PESs in each system, for each value of $r_{\rm CS}$ and $r_{\rm SiS}$ a different (optimized) 2D-set of data point locations $\{R_i;\theta_i\}$ was generated and used in the fit. In all cases, the PES-construction started with a seed-grid of 120 automatically (randomly) generated points, then 8 points were added to the fit on each iteration, improving the PES until the global RMS error was below 1 $\rm cm^{-1}$. In the next step, a focused refinement is made (adding 4 new points per iteration) until the RMS error was lower than 0.1 $\rm cm^{-1}$ for $R < 5.0$ Å and $E < E_{asymp}$. In total, 1618 (1771) points were needed for the complete representation of the Ar–CS (Ar–SiS) vdW interactions, with a RMS error of only 0.05 $\rm cm^{-1}$

TABLE I. Geometric parameters $(R, \theta)$ and potential energy $(V)$ for the global minimum of Ar–SiO($v$=0), Ar–CS($v$=0), Ar–SiS($v$=0) and Ar–CO($v$=0) vdW complexes. The barriers to linearity, both at the tetrel (C, Si, ...) end (t-barrier) and chalcogen (O, S, ...) end (c-barrier) are also shown. Units are Angströms, degrees, and cm$^{-1}$.

| | Ar–SiO[a] | Ar–CS | Ar–SiS | Ar–CO[b] |
|---|---|---|---|---|
| $R$ | 3.814 | 3.989 | 4.060 | 3.714 |
| $\theta$ | 89.5 | 111.3 | 104.2 | 92.88 |
| $V$ | -152.31 | -135.99 | -160.06 | -104.68 |
| c-barrier | 7.20 | 12.89 | 34.98 | 19.65 |
| t-barrier | 66.68 | 39.73 | 68.30 | 31.32 |

[a] Reference[6]

[b] Reference[2]

(0.06 cm$^{-1}$) for energy-regions below the asympote. The analytical representation of each PES is available from the authors upon request.

By appropriately weighting (combining) the eight PESs according to the PO-DVR coefficients (*cf.* equation 2), PESs vibrationally averaged over the probability densities were obtained for both Ar–CS($v = 0, 1, \cdots, 3$) and Ar–SiS($v = 0, 1, \cdots, 3$) systems. The geometric parameters and potential energy for the global minimum of Ar–CS($v = 0$) and Ar–SiS($v = 0$) vdW complexes are shown in Table I; for comparison, the corresponding values for Ar–SiO and Ar–CO systems are also provided in the table. The $v = 0$ PESs are compared in Figure 2, including also the previously studied Ar–SiO system, whose well-depth of 152 cm$^{-1}$ is between the other two. The value of $\theta = 180^\circ$ in the figure represents a colinear arrangement, with Ar associated at the tetrel end of the diatom (C or Si), whereas $\theta = 0^\circ$ places the Ar-atom at the chalcogen end (O or S). The barriers to linearity, both at the tetrel end (t-barrier) and chalcogen end (c-barrier) are given in Table I. Considering also CO, despite notable differences in the electronic structures of the four isovalent diatomics, their Ar-complexes all have global minima with nearly T-shaped ($\theta = 90^\circ$) geometries.

Figure 3 compares the minimum energy paths along $\theta$ for the SiO, CS, and SiS systems. The largest barrier to linearity is consistently the tetrel end of the molecules (this is true also for CO), and similar barriers are found for the two Si containing systems. For CO that

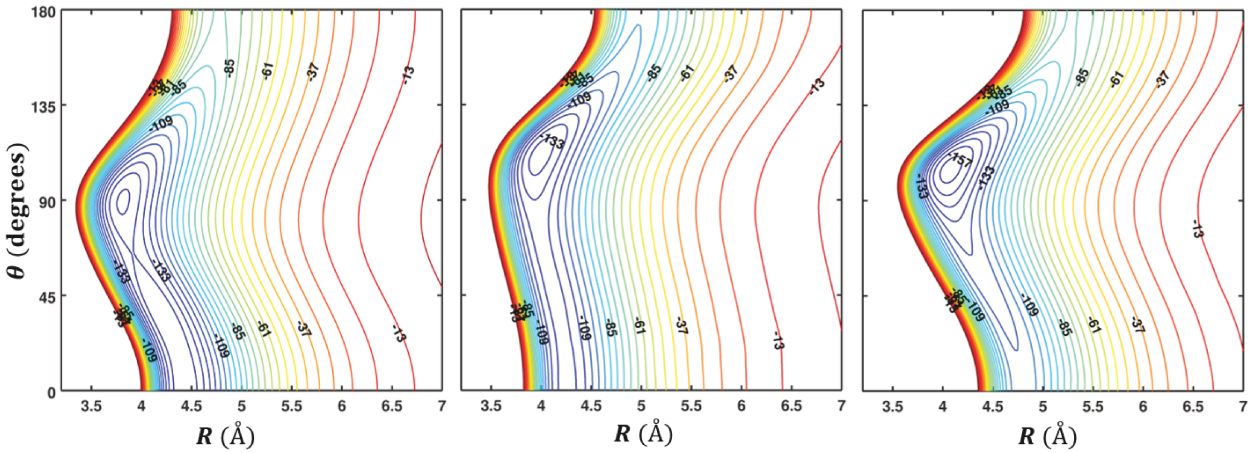


FIG. 2. Plot of the vdW interaction potential. Left: Ar–SiO($v$=0). Center: Ar–CS($v$=0). Right: Ar–SiS($v$=0). Contour values represent interaction energies in cm$^{-1}$.

barrier has been reported at around 31 cm$^{-1}$ (relative to a well depth of 105 cm$^{-1}$), which is similar to that barrier in the CS system reported here. The behavior at the chalcogen end is more interesting. SiS and CO are each composed of elements of the same row and the barrier to linearity at the chalcogen end is also significant, and thus provides a well that will effectively confine the wave functions of the complex. CS and SiO are each unbalanced (in the sense of coming from different rows of the periodic table) in opposite directions, and SiO is the odd one out from this set of four. Indeed, as previously reported, the wave function (beyond a very small barrier that is well below the zero-point-energy) is free to explore a long channel all the way to linearity. In fact, despite the minimum appearing near 90 degrees, the probability density accumulates mostly towards linearity. This behavior, which influences the geometries of the complexes as well as the dipole moments of the diatomics, has significant consequences for measured spectra. The magnitude of the complex dipole and its alignment with the inertial axes dictates the intensity of microwave transitions. In these systems, T-shaped complexes will tend to have $b$-type transitions with the most significant intensity, while closer to linear complexes will exhibit stronger $a$-type transitions. This was seen in Ar–SiO, which has very strong $a$-type transitions due to both the large dipole moment of SiO and its alignment in the nearly linear complex. It would be interesting to explore whether GeS and SeSi continue this pattern (with GeS perhaps having a low energy channel, while SeSi may not).

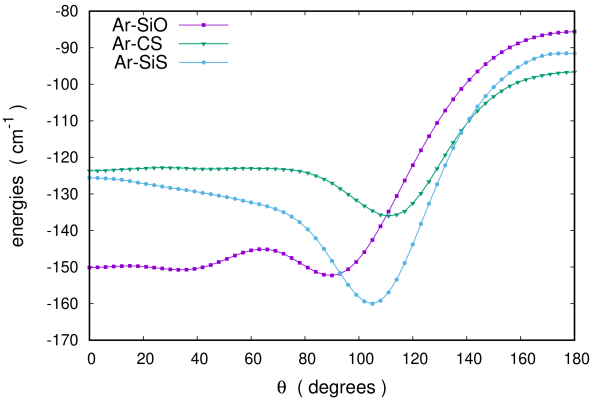


FIG. 3. Minimum energy paths along coordinate $\theta$ for the Ar–SiO, Ar–CS, and Ar–SiS systems.

### B. Theoretically predicted transitions

For each vibrational quantum number of the diatom $v$, a separate series of calculations were performed to compute the vdW rovibrational states. The $J = 0$ levels are only of even parity, while both even and odd-parity levels exist for $J > 0$. Wavefunctions and probability densities were computed in order to assign the states. A series of predicted transitions were determined by considering energy differences between states which involve $\Delta J = \pm 1$ and a switch in parity. Once completed, and the transition frequencies tabulated, the full 3D results are compared with those of the 2D vibrationally averaged ($v = 0$) PES. The vibrational averaging approximation is so accurate in these cases that differences of only 4–6 MHz are recorded. Those differences are retained as shifts to be applied to the rest of the progression of results for $v > 0$.

The assignment of each rovibrational level was done by visual inspection of the probability density plots for each state. The first lower states, are straightforward to assign, but the assignment becomes more complicated for higher lying states (as can be seen in the SI, Figures S1 and S2). Probability density plots corresponding to the lowest three vdW levels for $J = 0$ are shown in Figure 4. The first few levels correspond to excitation of the vdW bending mode, with nodes and delocalization appearing along the angle coordinate. For the Ar–CS system, the wave function is only localized near T-shaped ($\theta = 90°$) for the ground state, above which it explores a wide range of angles. For the bend-excited states, as in the Ar–SiO system, despite the global minimum appearing near 90 degrees, the probability

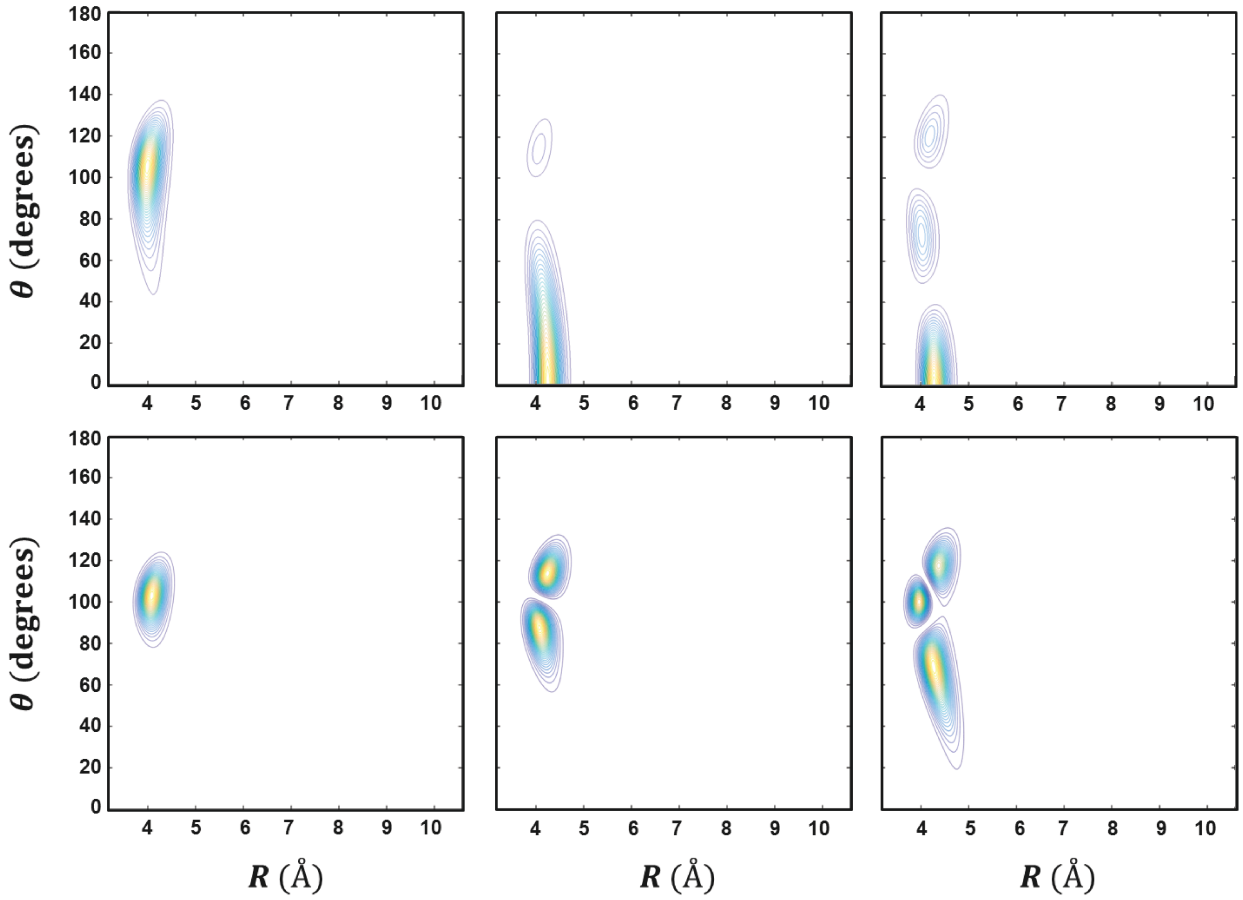


FIG. 4. Probability density plots corresponding to the three lowest $J = 0$ vdW states for Ar–CS (upper panels) and Ar–SiS (lower panels) vdW systems. The two systems exhibit somewhat different degrees of delocalization along $\theta$ as governed by the PESs (see text).

density accumulates mostly towards linearity.

Table II provides the calculated $a$-type rotational transition frequencies of Ar–CS and Ar–SiS without diatom vibrational excitation ($v = 0$). The rest of the computed $a$- and $b$-type transition frequencies—for both systems—as a function of diatom vibrational quantum number $v = 0$–3 , are reported in the SI, Tables S5–S8.

### C. Experimental results

Figure 5 compares two spectra collected under nearly identical conditions, the first one using Ar as the buffer gas and the second one using Ne. The most prominent features in

TABLE II. Theoretical frequencies of normal Ar–CS and Ar–SiS in the $v = 0$ stretching and excited bending mode (in MHz).

| Transition: $J'_{K'_a,K'_c} \rightarrow J_{K_a,K_c}$ | Ar–CS | Ar–SiS |
|---|---|---|
| $(\Delta J = 1, K_a = 0, K_c = J)$ | | |
| $1_{0,1} \rightarrow 0_{0,0}$ | 2879.79 | 2323.21 |
| $2_{0,2} \rightarrow 1_{0,1}$ | 5758.77 | 4644.20 |
| $3_{0,3} \rightarrow 2_{0,2}$ | 8636.12 | 6960.75 |
| $4_{0,4} \rightarrow 3_{0,3}$ | 11511.02 | 9270.65 |
| $5_{0,5} \rightarrow 4_{0,4}$ | 14382.65 | 11571.74 |
| $6_{0,6} \rightarrow 5_{0,5}$ | 17250.15 | 13861.96 |
| $7_{0,7} \rightarrow 6_{0,6}$ | 20112.68 | 16139.38 |
| $8_{0,8} \rightarrow 7_{0,7}$ | 22969.36 | 18402.33 |
| $9_{0,9} \rightarrow 8_{0,8}$ | 25819.30 | 20649.49 |
| $(\Delta J = 1, K_a = 1, K_c = J)$ | | |
| $2_{1,2} \rightarrow 1_{1,1}$ | 5616.83 | 4494.42 |
| $3_{1,3} \rightarrow 2_{1,2}$ | 8424.16 | 6739.88 |
| $4_{1,4} \rightarrow 3_{1,3}$ | 11230.17 | 8983.28 |
| $5_{1,5} \rightarrow 4_{1,4}$ | 14034.44 | 11223.94 |
| $6_{1,6} \rightarrow 5_{1,5}$ | 16836.50 | 13461.25 |
| $7_{1,7} \rightarrow 6_{1,6}$ | 19635.93 | 15694.63 |
| $8_{1,8} \rightarrow 7_{1,7}$ | 22432.27 | 17923.53 |
| $9_{1,9} \rightarrow 8_{1,8}$ | 25225.07 | 20147.46 |
| $(\Delta J = 1, K_a = 1, K_c = J - 1)$ | | |
| $2_{1,1} \rightarrow 1_{1,0}$ | 5846.33 | 4795.18 |
| $3_{1,2} \rightarrow 2_{1,1}$ | 8767.90 | 7190.79 |
| $4_{1,3} \rightarrow 3_{1,2}$ | 11687.56 | 9584.01 |
| $5_{1,4} \rightarrow 4_{1,3}$ | 14604.66 | 11973.99 |
| $6_{1,5} \rightarrow 5_{1,4}$ | 17518.55 | 14359.87 |
| $7_{1,6} \rightarrow 6_{1,5}$ | 20428.55 | 16740.76 |
| $8_{1,7} \rightarrow 7_{1,6}$ | 23333.99 | 19115.72 |
| $9_{1,8} \rightarrow 8_{1,7}$ | 26234.16 | 21483.74 |
| **Bend Excited State:** | | |
| $(\Delta J = 1, K_a = 0, K_c = J)$ | | |
| $1_{0,1} \rightarrow 0_{0,0}$ | 2671.90 | 2278.57 |
| $2_{0,2} \rightarrow 1_{0,1}$ | 5343.50 | 4554.39 |
| $3_{0,3} \rightarrow 2_{0,2}$ | 8014.51 | 6824.72 |
| $4_{0,4} \rightarrow 3_{0,3}$ | 10684.61 | 9086.79 |
| $5_{0,5} \rightarrow 4_{0,4}$ | 13353.48 | 11337.87 |
| $6_{0,6} \rightarrow 5_{0,5}$ | 16020.82 | 13575.27 |
| $7_{0,7} \rightarrow 6_{0,6}$ | 18686.33 | 15796.51 |
| $8_{0,8} \rightarrow 7_{0,7}$ | 21349.75 | 17999.39 |
| $9_{0,9} \rightarrow 8_{0,8}$ | 24010.92 | 20182.19 |

both spectra arise from normal, isotopic, and vibrationally excited SiS between ∼17,500 and 18,100 MHz[39] and were assigned using catalog entries in the Cologne Database for Molecular Spectroscopy.[42] Rotational transitions from vibrational states up to $v = 18$ (corresponding to over 12,000 K of vibrational energy), were observed with good signal-to-noise ratio (SNR). Other abundantly produced molecules in this gas mixture which give rise to strong lines include the well-known carbon-sulfur chains such as CCS and CCCS[35], indicated in Figure 5(b). Figure 5(c) displays spectral features in the Ar spectrum after removing rotational lines of known molecules. Presumably, the remaining transitions arise from molecules whose rotational spectra have not been reported previously. Here, only the most abundant isotopes were assigned unambiguously. In addition to two features near ∼15,900 MHz, the blue shaded regions in panel (c) highlight strong features that are entirely absent in the Ne discharge, and therefore almost certainly arise from one or more Ar-bearing species.

Guided by the theoretical predictions of Ar–SiS (Table II), the strongest transitions in Figure 5(c) were investigated further. Figure 6 shows several narrow frequency slices of the full spectrum in which each slice is centered on the predicted frequency for five successive *b*-type ($\Delta J = 1$, $\Delta K_a = +1$, $\Delta K_c = -1$) transitions—three of which correspond to the strong features highlighted in Figure 5(c). As can be seen in Figure 6, a feature close in frequency to the theoretical prediction is present in each spectrum. Owing to the nonlinear instrument-response of our spectrometer, however, there is considerable intensity variation in these spectra. If the instrument response was perfectly flat, the relative intensities of successive transitions should follow a Boltzmann distribution with $T_{rot} \sim 2$ K.

Each transition in the broadband spectrum was subsequently re-measured at higher spectral resolution using a cavity microwave spectrometer. The resulting frequencies together with the theoretical assignments were used as input to an *A*-reduced asymmetric top Hamiltonian[43,44] using the SPFIT program.[45] From this preliminary fit neighboring *b*-type transitions were then predicted, namely those with the selection rules $\Delta J = 1, \Delta K_a = +1, \Delta K_c = +1$,[46] of which four fall within the range of our spectrometer. With six free parameters ($A, B, C$, and quartic centrifugal distortion terms $\Delta_J, \Delta_{JK}, \delta_J$) we obtain a RMS error of 24 kHz. The relatively large fitting error (compared to other high-resolution microwave studies) is not surprising, since a weakly-bound complex has a non-rigid structure and large vibration-rotation interaction; both of which are poorly treated by our effective Hamiltonian. Comparison with the related Ar−SiO molecule, however, shows that this effect is much more

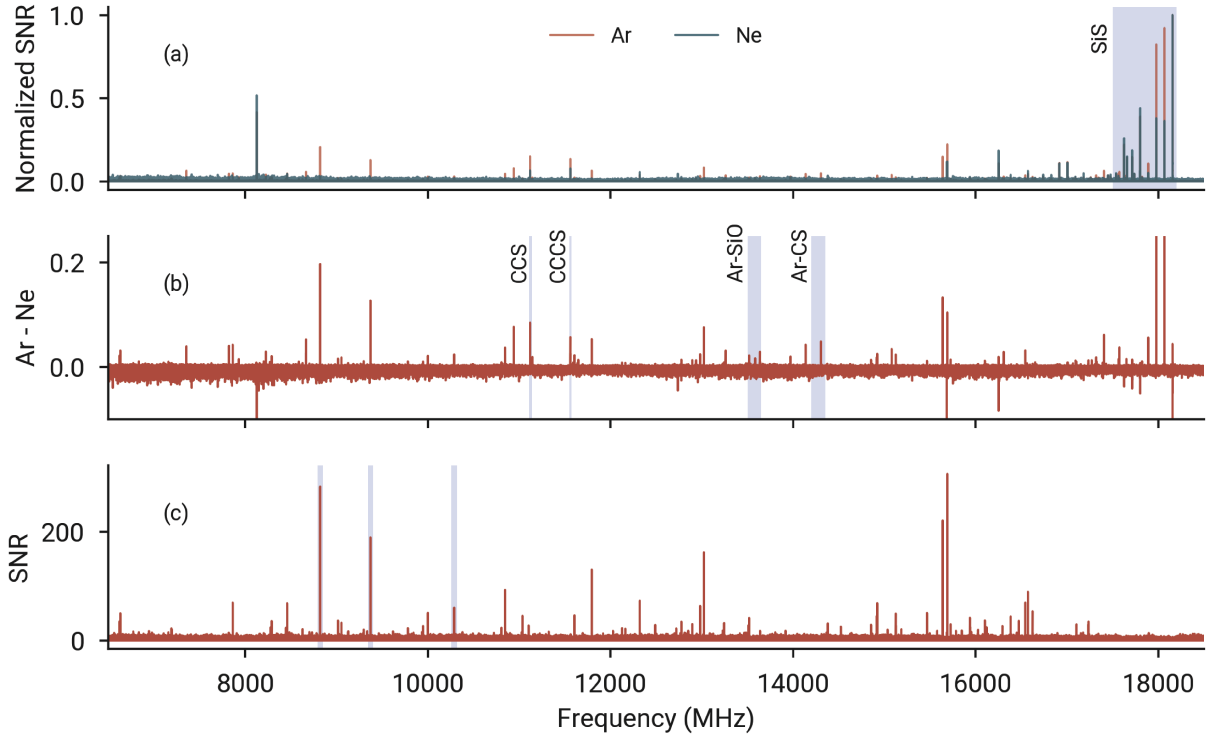


FIG. 5. Comparison of broadband chirped-pulse spectra collected with Ne and Ar buffer gases, using the same dilute gas mixture ($CS_2 + SiH_4$). The top trace (a) shows the two spectra overlaid, while (b) shows the residual of Ar spectrum following subtraction of the Ne spectrum. Several well-known species are highlighted in (a) and (b). The bottom trace (c) shows the Ar spectrum (in SNR units), in which transitions of known species have been removed; three strong features that are not present in Ne spectrum are highlighted.

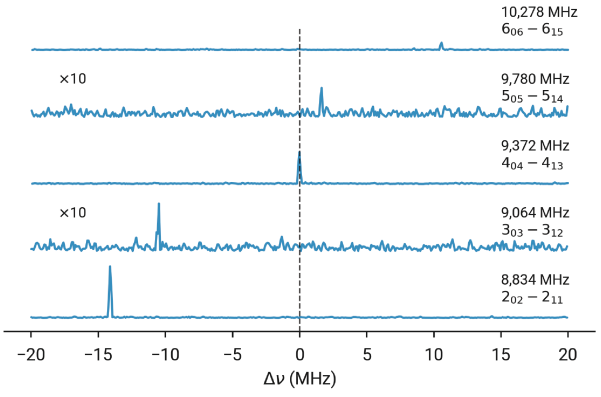


FIG. 6. Spectral slices of Figure 5, where the frequency axis of each slice is offset by the predicted theoretical transition frequency for five successive *b*-type transitions.

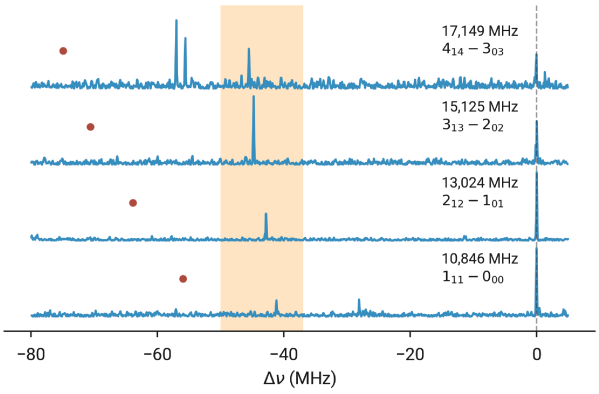


FIG. 7. Loomis-Wood plot showing selected regions of the broadband spectrum near the strong *b*-type transitions of ground state Ar−SiS. Red scatter points indicate the predicted transition frequencies of Ar−SiS($v = 1$) from the theoretical calculation.

pronounced for Ar−SiO than for Ar−SiS, which reinforces the fact that the latter is much more confined by the PES (see Figure 2).

Having confidently detected rotational transitions of Ar−SiS, we then proceeded to search for evidence of vibrationally excited states, guided once again by the theoretical predictions. Figure 7 shows a simplified Loomis-Wood visualization, where each trace is a small portion of the wider broadband spectrum, and is plotted relative to the frequency of a *b*-type transition of ground state Ar−SiS for four successive transitions. As highlighted in orange, a series of lines with nearly the same frequency offset from the $v = 0$ lines are clearly visible; these lines were ultimately assigned to the $v = 1$ state of Ar−SiS. The theoretical predictions reproduce not only the absolute frequency shifts but also the effect of centrifugal distortion with increasing $J$—the frequency shifts in Figure 7 appear to be mostly a systematic offset from the experimentally observed transitions. With these preliminary assignments in hand, we performed a similar nonlinear least squares optimization as was done for the vibrational ground state to fit and predict additional lines. Table III summarizes the best-fit constants which reproduce the experimental frequencies with a fit RMS error (3 kHz) comparable to the measurement uncertainty (2–5 kHz).

The $B$ and $C$ rotational constants in $v = 0$ and $v = 1$ are very similar, while $A$ decreases slightly (by 0.5%) when vibrational energy is imparted into the SiS, consistent with the motion effectively localized between Ar and SiS. Using a simplified mechanical model, comparison of the centrifugal distortion and rotational constants provides a way to mea-

TABLE III. Best-fit spectroscopic constants (in MHz) of Ar−SiS in $v = 0$ and $v = 1$. An $A$-reduced representation was used; values in parentheses correspond to $1\sigma$ uncertainties.

| Parameter | $v = 0$ | $v = 1$ |
|---|---|---|
| $A$ | 9757.1084(33) | 9717.2228(133) |
| $B$ | 1242.3389(68) | 1242.799(86) |
| $C$ | 1089.92323(96) | 1089.0487(119) |
| $\Delta_J \times 10^3$ | 3.4204(112) | 7.74(125) |
| $\Delta_{JK}$ | 0.26631(146) | 0.4944(145) |
| $\Delta_K \times 10^3$ | 1.1289(71) | 1.53(48) |

sure the rigidity of the molecule[37,47]—in this case, we compute $\log \frac{\Delta_J}{(B+C)/2}$, the values of which are −6.13 and −5.78 for $v = 0$ and $v = 1$ respectively. In this picture, the complex becomes less rigid and therefore less strongly bound: progressing from something akin to $H_2O$−$HC_4H$ (−6.4)[48] to Ar−$HC_4H$ (−5.2).[49] For additional context, in our earlier investigation of Ar−SiO,[37] we determine $\log \frac{\Delta_J}{(B+C)/2}$ values of −4.09 and −4.05 for $v = 0$ and $v = 1$ respectively, implying a significantly more delocalized complex than the present case of Ar−SiS. Additionally, vibrational excitation does not significantly affect the binding of Ar−SiO, whereas for Ar−SiS, we obtain a larger degree of rigidity change going from $v = 0$ to $v = 1$. All of these experimental observations suggest that the Ar−SiS structure is much more rigidly bound than that of Ar−SiO. This is certainly true as can be seen in plots of the PESs (Figure 2). Note however, that as given in Table I, the absolute binding energy for Ar−SiS is only very slightly greater than for Ar−SiO (−160 $cm^{-1}$ compared with −152 $cm^{-1}$). The key difference is the degree of angular confinement, which is clear from the plot of minimum energy paths for cuts through $\theta$, given in Figure 3. The dramatic difference comes from the S atom since as given in Table I, the barriers to linearity at the Si end of the molecules are nearly identical, whereas at the chalcogen end (O or S), the barriers differ greatly. Thus, despite similar binding energies of the two complexes, due to lack of angular confinement, Ar−SiO is much floppier. This makes Ar−SiS less sensitive and easier to predict accurately. Table IV provides a comparison of the calculated and measured $b$-type transition frequencies for the Ar–SiS complex, for both $v = 0$ and $v = 1$ vibrational quanta in the Si–S stretch. In all cases, agreement between theory and experiment is excellent, with deviations in frequency no worse than 0.19 % over the range of measurements.

Figure 8 displays the original broadband spectrum recorded with Ar as a buffer gas,

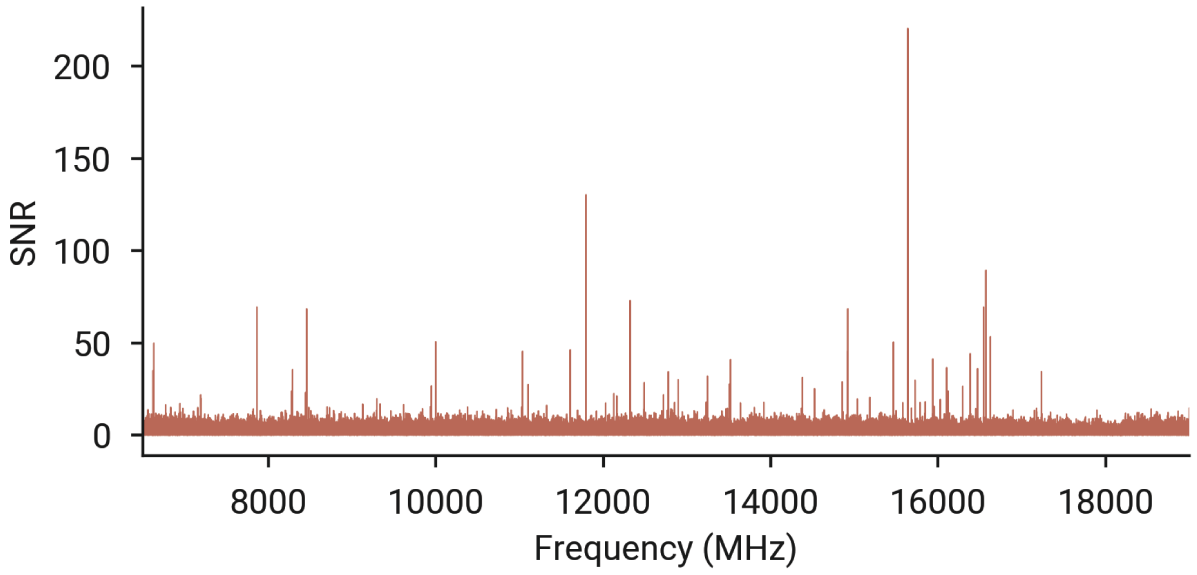


FIG. 8. A re-plot of the Ar spectrum in Figure 5 after removing all assigned lines.

replotting Figure 5(c), but with the newly assigned lines of Ar−SiS removed. Not surprisingly many features, some with high SNR, remain. Based on our previous Ar *versus* Ne comparison, these lines very likely arise from other Ar-bearing complexes, many of which are probably entirely new. In light of the present work, identifying the carriers of the unassigned features in Figure 8 may be relatively straightforward, since the present *ab initio* calculations were able to predict the rotational spectrum of weakly-bound complexes from first principles—and in an automated fashion—that are in quantitative agreement with the experimental findings. The only remaining puzzle would appear to be knowledge of the most abundant product species in a $SiH_4/CS_2$ discharge.

## V. SUMMARY AND CONCLUSIONS

We presented in this paper a combined theoretical/experimental study of the rotational spectra of Ar–CS($v$) and Ar–SiS($v$) complexes, further demonstrating that the simplified approach of making a series of vibrationally effective PESs for the intermolecular coordinates (one for each reaction-product quantum number of interest) can quantitatively predict the vdW energy levels for the complex with spectroscopic accuracy. Indeed, in this study the calculations preceded the measurements, and as seen in Table IV, many of the predictions

TABLE IV. Comparison of observed (Expt) and predicted (Calc) $b$-type transition frequencies for the Ar–SiS complex (in MHz). The value of the difference ($\Delta$ = Calc − Expt, in MHz) and percentage deviation (% dev) between theory and experiment is also shown.

| | $J'_{K'_a,K'_c} - J''_{K''_a,K''_c}$ | **Expt** | **Calc** | $\Delta$ | **% dev** |
|---|---|---|---|---|---|
| $v = 0$ | $1_{1,0} \rightarrow 1_{0,1}$ | 8666.6390 | 8683.14 | -16.50 | 0.19 |
| | $2_{1,1} \rightarrow 2_{0,2}$ | 8819.9866 | 8834.12 | -14.14 | 0.16 |
| | $3_{1,2} \rightarrow 3_{0,3}$ | 9053.7244 | 9064.17 | -10.45 | 0.12 |
| | $4_{1,3} \rightarrow 4_{0,4}$ | 9372.2782 | 9377.53 | -5.25 | 0.06 |
| | $5_{1,4} \rightarrow 5_{0,5}$ | 9781.4444 | 9779.78 | 1.67 | 0.02 |
| | $6_{1,5} \rightarrow 6_{0,6}$ | 10288.2840 | 10277.69 | 10.59 | 0.10 |
| | $1_{1,1} \rightarrow 0_{0,0}$ | 10846.4045 | 10855.93 | -9.52 | 0.09 |
| | $2_{1,2} \rightarrow 1_{0,1}$ | 13024.0708 | 13027.13 | -3.06 | 0.02 |
| | $3_{1,3} \rightarrow 2_{0,2}$ | 15124.5950 | 15122.82 | 1.78 | 0.01 |
| | $4_{1,4} \rightarrow 3_{0,3}$ | 17149.1796 | 17145.35 | 3.83 | 0.02 |
| $v = 1$ | $1_{1,0} \rightarrow 0_{0,0}$ | 8627.1837 | 8619.15 | 8.03 | 0.09 |
| | $2_{1,1} \rightarrow 1_{0,1}$ | 8780.9800 | 8771.03 | 9.95 | 0.11 |
| | $3_{1,2} \rightarrow 2_{0,2}$ | 9015.4477 | 9002.49 | 12.96 | 0.14 |
| | $4_{1,3} \rightarrow 3_{0,3}$ | 9335.1100 | 9317.86 | 17.25 | 0.18 |
| | $1_{1,1} \rightarrow 0_{0,0}$ | 10805.2579 | 10790.44 | 14.82 | 0.14 |
| | $2_{1,2} \rightarrow 1_{0,1}$ | 12981.2102 | 12960.16 | 21.05 | 0.16 |
| | $3_{1,3} \rightarrow 2_{0,2}$ | 15079.8294 | 15053.96 | 25.87 | 0.17 |
| | $4_{1,4} \rightarrow 3_{0,3}$ | 17103.6673 | 17084.25 | 19.42 | 0.11 |

were accurate enough to guide highly focused searches for signals from the spectrometer. This was possible because the calculations are sufficiently accurate and from first principles, without needing empirical adjustment.

Similar future studies can be easily conducted using our freely available PES-fitting code AUTOSURF. We have described in detail the methodology of our approach—from the automated construction of the necessary PESs to the variational calculations of the unbound metastable states—which can be generally applied to any vdW complex formed by a rare gas atom C and a more strongly-bound diatomic molecule AB, to predict from first principles the rotational spectrum of such weakly-bound complexes in an automated fashion.

The applications of this study are the Ar–CS and Ar–SiS complexes, which are isovalent to Ar–CO and Ar–SiO, the latter of which we considered in a previously reported study. The convenience of our automated approach going forward is that it enables one to study entire families or sets of slightly differing species simultaneously with sufficient accuracy to be useful to experimentalists.

## VI. SUPPORTING INFORMATION

Additional details of the calculations are supplied as Supporting Information. This includes the precise points and weights for the DVR calculations, additional tables of predicted transitions, and the SPFIT output for the analysis of experimental data.

## VII. ACKNOWLEDGMENTS

R.D. is supported by the U.S. Department of Energy, Office of Science, Office of Basic Energy Sciences (Award DE-SC0019740). M.C.M. is supported by the U.S. National Science Foundation (NSF CHE-1566266).

[1] Martina Havenith and Gerhard W. Schwaab, "Attacking a small beast: Ar–CO, a prototype for intermolecular forces," Zeitschrift für Physikalische Chemie **219**, 1053–1088 (2009).

[2] Rafał R. Toczyłowski and Sławomir M. Cybulski, "An ab initio study of the potential energy surface and spectrum of Ar–CO," The Journal of Chemical Physics **112**, 4604–4612 (2000).

[3] Yunjie Xu and A. R. W. McKellar, "The infrared spectrum of the Ar-CO complex. Comprehensive analysis including van der Waals stretching and bending states," Molecular Physics **88**, 859–874 (1996).

[4] L. H. Coudert, I. Pak, and L. Surin, "The potential energy surface of the Ar–CO complex obtained using high-resolution data," The Journal of Chemical Physics **121**, 4691–4698 (2004).

[5] Yoshihiro Sumiyoshi and Yasuki Endo, "Three-dimensional potential energy surface of Ar–CO," The Journal of Chemical Physics **142**, 024314 (2015).

[6] Michael C McCarthy, Steve Alexandre Ndengué, and Richard Dawes, "The rotational spectrum and potential energy surface of the Ar–SiO complex," The Journal of Chemical Physics **149**, 134308 (2018).

[7] Ohnaka, K., "High spectral resolution spectroscopy of the SiO fundamental lines in red giants and red supergiants with VLT/VISIR," Astronomy and Astrophysics **561**, A47 (2014).

[8] W. D. Cotton, W. Vlemmings, B. Mennesson, G. Perrin, V. Coudé du Foresto, G. Chagnon, P. J. Diamond, H. J. van Langevelde, E. Bakker, and S. Ridgway *et al.*, "Further VLBA

observations of SiO masers toward mira variable stars," Astronomy and Astrophysics **456**, 339–350 (2006).

[9] Fredrik L. Schöier, David Fong, Hans Olofsson, Qizhou Zhang, and Nimesh Patel, "The distribution of SiO in the circumstellar envelope around IRC +10216," The Astrophysical Journal **649**, 965 (2006).

[10] Makoto Miyoshi, Kin'ya Matsumoto, Seiji Kameno, Hiroshi Takaba, and Takahiro Iwata, "Collisional pumping of SiO masers in evolved stars," Nature **371**, 395–397 (1994).

[11] T. Kamiński, C. A. Gottlieb, K. H. Young, K. M. Menten, and N. A. Patel, "An interferometric spectral line and imaging survey of VY canis majoris in the 345 GHz band," The Astrophysical Journal Supplement Series **209**, 38 (2013).

[12] James F Harrison, "Relationship between the charge distribution and dipole moment functions of CO and the related molecules CS, SiO, and SiS," The Journal of Physical Chemistry A **110**, 10848–10857 (2006).

[13] John W. Raymonda, John S. Muenter, and William A. Klemperer, "Electric dipole moment of SiO and GeO," The Journal of Chemical Physics **52**, 3458–3461 (1970).

[14] J. S. Muenter, "Electric dipole moment of carbon monoxide," Journal of Molecular Spectroscopy **55**, 490–491 (1975).

[15] Jonathan Tennyson, "The calculation of the vibration-rotation energies of triatomic molecules using scattering coordinates," Computer Physics Reports **4**, 1–36 (1986).

[16] Z Bacić and JC Light, "Highly excited vibrational levels of "floppy" triatomic molecules: A discrete variable representation—distributed gaussian basis approach," The Journal of Chemical Physics **85**, 4594–4604 (1986).

[17] Z Bačić and JC Light, "Accurate localized and delocalized vibrational states of HCN/HNC," The Journal of Chemical Physics **86**, 3065–3077 (1987).

[18] Zlatko Bačić and John C Light, "Theoretical methods for rovibrational states of floppy molecules," Annual Review of Physical Chemistry **40**, 469–498 (1989).

[19] H. Wei and T. Carrington, "The discrete variable representation of a triatomic Hamiltonian in bond length-bond angle coordinates," The Journal of Chemical Physics **97**, 3029 (1992).

[20] Jeremy M Hutson, "Vibrational dependence of the anisotropic intermolecular potential of Ar–HF," The Journal of Chemical Physics **96**, 6752–6767 (1992).

[21] Suyan Liu, Zlatko Bačić, Jules W Moskowitz, and Kevin E Schmidt, "Isomer dependence of HF vibrational frequency shift for $Ar_nHF$ (n= 4–14) van der waals clusters: Quantum five-dimensional bound state calculations," The Journal of Chemical Physics **103**, 1829–1841 (1995).

[22] Michael Von Dirke, Zlatko Bačić, Dong H Zhang, and John ZH Zhang, "Vibrational predissociation of HF dimer in $\nu$HF= 1: Influence of initially excited intermolecular vibrations on the fragmentation dynamics," The Journal of Chemical Physics **102**, 4382–4389 (1995).

[23] Ernesto Quintas-Sánchez and Richard Dawes, "AUTOSURF: A freely available program to construct potential energy surfaces," Journal of Chemical Information and Modeling **59**, 262–271 (2019).

[24] Moumita Majumder, Steve Alexandre Ndengué, and Richard Dawes, "Automated construction of potential energy surfaces," Molecular Physics **114**, 1–18 (2016).

[25] Richard Dawes and Ernesto Quintas-Sánchez, "The Construction of Ab Initio-Based Potential Energy Surfaces," in *Reviews in Computational Chemistry vol. 31* (John Wiley & Sons, Inc., 2018) Chap. 5, pp. 199–264.

[26] H. Werner, P. Knowles, G. Knizia, F. Manby, M. Schütz, P. Celani, T. Korona, R. Lindh, A. Mitrushenkov, and G. Rauhut *et al.*, "Molpro, version 2012.1, a package of ab initio programs," (2012), see http://www.molpro.net.

[27] Richard Dawes and Steve A Ndengué, "Single-and multireference electronic structure calculations for constructing potential energy surfaces," International Reviews in Physical Chemistry **35**, 441–478 (2016).

[28] Steve Ndengué, Richard Dawes, Xiao-Gang Wang, Tucker Carrington Jr, Zhigang Sun, and Hua Guo, "Calculated vibrational states of ozone up to dissociation," The Journal of Chemical Physics **144**, 074302 (2016).

[29] Gordon G. Brown, Brian C. Dian, Kevin O. Douglass, Scott M. Geyer, Steven T. Shipman, and Brooks H. Pate, "A broadband Fourier transform microwave spectrometer based on chirped pulse excitation," Review of Scientific Instruments **79**, 053103 (2008).

[30] T. J. Balle and W. H. Flygare, "Fabry–Perot cavity pulsed Fourier transform microwave spectrometer with a pulsed nozzle particle source," Review of Scientific Instruments **52**, 33–45 (1981).

[31] Kyle N. Crabtree, Oscar Martinez, and Michael C. McCarthy, "Detection of two highly stable silicon nitrides: HSiNSi and $H_3SiNSi$," The Journal of Physical Chemistry A **117**, 11282–11288 (2013).

[32] Kyle N. Crabtree, Marie-Aline Martin-Drumel, Gordon G. Brown, Sydney A. Gaster, Taylor M. Hall, and Michael C. McCarthy, "Microwave spectral taxonomy: A semi-automated combination of chirped-pulse and cavity fourier-transform microwave spectroscopy," The Journal of Chemical Physics **144**, 124201 (2016).

[33] M.C. McCarthy and P. Thaddeus, "Geometrical structure of monobridged disilyene Si(H)SiH," Journal of Molecular Spectroscopy **222**, 248–254 (2003).

[34] Michael C. McCarthy and Jürgen Gauss, "Exotic $SiO_2H_2$ isomers: Theory and experiment working in harmony," The Journal of Physical Chemistry Letters **7**, 1895–1900 (2016).

[35] Brett A. McGuire, Marie-Aline Martin-Drumel, Kin Long Kelvin Lee, John F. Stanton, Carl A. Gottlieb, and Michael C. McCarthy, "Vibrational satellites of $C_2S$, $C_3S$, and $C_4S$: microwave spectral taxonomy as a stepping stone to the millimeter-wave band," Physical Chemistry Chemical Physics **20**, 13870–13889 (2018).

[36] M. Eugenia Sanz, Michael C. McCarthy, and Patrick Thaddeus, "Vibrational excitation and relaxation of five polyatomic molecules in an electrical discharge," The Journal of Chemical Physics **122**, 194319 (2005).

[37] Michael C. McCarthy, Steve Alexandre Ndengué, and Richard Dawes, "The rotational spectrum and potential energy surface of the Ar–SiO complex," The Journal of Chemical Physics **149**, 134308 (2018).

[38] Chisato Niida, Masakazu Nakajima, Yoshihiro Sumiyoshi, Yasuhiro Ohshima, Hiroshi Kohguchi, and Yasuki Endo, "Fourier-transform microwave spectroscopy and determination of the three dimensional potential energy surface for Ar–CS," The Journal of Chemical Physics **140**, 104310 (2014).

[39] H. S. P. Müller, M. C. McCarthy, L. Bizzocchi, H. Gupta, S. Esser, H. Lichau, M. Caris, F. Lewen, J. Hahn, and C. Degli Esposti *et al.*, "Rotational spectroscopy of the isotopic species of silicon monosulfide, SiS," Physical Chemistry Chemical Physics **9**, 1579–1586 (2007).

[40] Kin Long Kelvin Lee, "PySpecTools," (2020), 10.5281/zenodo.3662698.

[41] Kin Long Kelvin Lee and Michael McCarthy, "Study of benzene fragmentation, isomerization, and growth using microwave spectroscopy," The Journal of Physical Chemistry Letters **10**,

2408–2413 (2019).

[42] Christian P. Endres, Stephan Schlemmer, Peter Schilke, Jürgen Stutzki, and Holger S. P. Müller, "The Cologne database for molecular spectroscopy, CDMS, in the virtual atomic and molecular data center, VAMDC," Journal of Molecular Spectroscopy New Visions of Spectroscopic Databases, Volume II, **327**, 95–104 (2016).

[43] James K. G. Watson, "The vibration-rotation Hamiltonian of linear molecules," Molecular Physics **19**, 465–487 (1970).

[44] James K. G. Watson, "Determination of centrifugal distortion coefficients of asymmetric-top molecules," The Journal of Chemical Physics **46**, 1935–1949 (1967).

[45] H. M. Pickett, "The fitting and prediction of vibration-rotation spectra with spin interactions," J. Mol. Spectrosc. **148**, 371–377 (1991).

[46] S. A. Cooke and P. Ohring, "Decoding pure rotational molecular spectra for asymmetric molecules," Journal of Spectroscopy **2013** (2013), article ID: 698392.

[47] P. Thaddeus, M. C. McCarthy, M. J. Travers, C. A. Gottlieb, and W. Chen, "New carbon chains in the laboratory and in interstellar space," Faraday Discussions **109**, 121–135 (1998).

[48] K Matsumura, F. J Lovas, and R. D Suenram, "Structures of the $NH_3$−HCCCCH and $H_2O$−HCCCCH complexes by Fourier-transform microwave spectroscopy," Journal of Molecular Spectroscopy **144**, 123–138 (1990).

[49] Keiji Matsumura, Yasuhiro Ohshima, and Yasuki Endo, "Fourier-transform microwave spectroscopy of the argon–diacetylene van der Waals complex," Journal of Molecular Spectroscopy **185**, 178–184 (1997).